Analytical Methods

ROYAL SOCIETY OF CHEMISTRY

PAPER

View Article Online
View Journal

Cite this: DOI: 10.1039/d2ay01040b

Nanoarchitectonics of neomycin-derived fluorescent carbon dots for selective detection of Fe^{3+} ions†

Ratan W. Jadhav, Pritesh P. Khobrekar, Sandesh T. Bugde and Sheshanath V. Bhosale *

The first-ever neomycin antibiotic-based carbon dots (Neo-CDs) were synthesized *via* a low-cost, eco-friendly, and single-step hydrothermal method using neomycin as a single precursor. The as-prepared Neo-CDs exhibited strong and stable blue fluorescence and were well characterized by TEM, UV-vis absorption, fluorescence emission, IR, XRD, Raman and XPS spectroscopy methods. The Neo-CDs showed a well-distributed size within the range of 4.5 to 7.8 nm, comprising various functional groups on the surface of the carbon core. The Neo-CDs exhibited exceptional emission behaviour, and fluorescence quantum yield was calculated to be 55% in double distilled water. Neo-CDs have been used as a fluorescent sensor for selective and sensitive detection of Fe^{3+} ions in aqueous solution in the fluorescence turn-off mode. From the set of metal ions, only the Fe^{3+} ion showed quenching of fluorescence due to photoinduced (PET) electron transfer from Neo-CDs to the half-filled 3d orbital of Fe^{3+} ions. The limit of detection for Fe^{3+} ions was calculated to be 0.854 μM. Further, the quenching efficiency and Stern–Volmer quenching constant have been calculated which are about 94% and 5.6×10^6 M^{-1}, respectively.

Received 28th June 2022
Accepted 23rd July 2022

DOI: 10.1039/d2ay01040b

rsc.li/methods

1. Introduction

Aminoglycoside antibiotics are an important class of antimicrobial drugs that are used for the treatment of both Gram-positive and Gram-negative bacterial infections. They have the ability to bind with 16S rRNA in the small ribosomal subunit of bacteria, causing interference in the translation process of protein synthesis, leading to bacterial death.[1–3] This class of antibiotics are naturally occurring aminoglycosides mainly consisting of kanamycin, neomycin, gentamycin and streptomycin. All the aminoglycoside antibiotics possess a common chemical structure which consists of aminocyclitol units with multiple amino and hydroxyl groups and saccharide units connected through glycosidic linkage.[4–7] The presence of multiple amino and hydroxyl groups in the aminoglycoside antibiotics allows biomaterial researchers to functionalize them with both covalent and non-covalent interactions for various biological applications.[8,9] In this study, we have synthesized carbon dots (CDs) using the neomycin antibiotic, as a single precursor.

In recent times, carbon dots (CDs) have attracted tremendous interest of researchers due to their unique optical properties, high water solubility, high biocompatibility, and low toxicity. They have applications in solar cells, photocatalysis and biological sciences, such as biological labelling, biosensing, bioimaging and for drug delivery. However, the low quantum yield of CDs is the major limitation to their applications.[10–17] In order to overcome this problem, many researchers have used the doping technique. Doping heteroatoms such as nitrogen and phosphorous into CDs leads to changes in their electronic properties and may create more active sites.[18–25] Thus, heteroatom doped CDs have been extensively synthesized to improve their electronic properties, quantum yield and photostability.

Various supramolecular sensors have been reported for the selective and sensitive detection of cations, anions and neutral species,[26] whereas in the past decade, designing and development of fluorescent CDs have become major interest of research due to their applications in sensing of biologically important metal ions. CDs have been employed for sensing of metal ions such as Fe^{3+} ions due to their high sensitivity, easy monitoring and rapid fluorescence response. The Fe^{3+} ion is one of the essential trace elements which plays an important role in cellular metabolism, oxygen transport in hemoglobin and as a cofactor in enzyme-catalysed reactions. Both deficiency and overdose of Fe^{3+} ions may cause serious damage to living cells, resulting in anaemia, arthritis, diabetes and heart failure, and

School of Chemical Sciences, Goa University, Taleigao Plateau, Goa-403 206, India. E-mail: svbhosale@unigoa.ac.in

† Electronic supplementary information (ESI) available: Synthetic characterisation and other details are available. See https://doi.org/10.1039/d2ay01040b

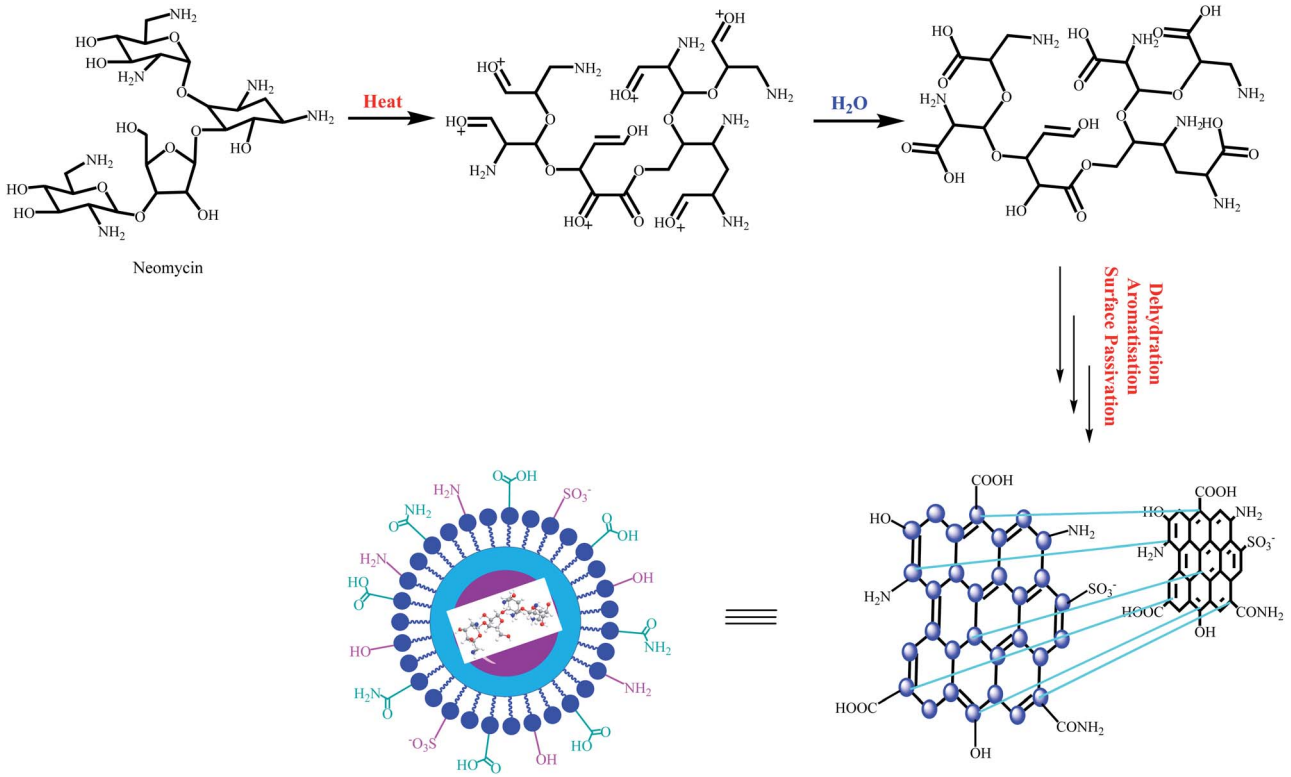

Scheme 1 Schematic representation for the synthesis of Neo-CDs.

therefore, the detection of Fe^{3+} ions is very important for diagnosis of these diseases. There are various qualitative and quantitative strategies that have been reported for the detection of Fe^{3+} ions, such as atomic absorption spectrometry, spectrophotometry, inductively coupled plasma mass spectrometry, voltammetry and fluorescence methods. Out of these, the fluorescence method is one of the easy, soft handling methods, whereas other methods require tedious sample preparation procedures and complicated instrumentation.[19,27–29]

Biomolecule derived CDs have been reported earlier for various applications.[14–17,30,31] The presence of multiple amino and hydroxyl groups in the neomycin antibiotic inspired us to synthesize its carbon nanomaterials. In this work, a green and facile hydrothermal strategy was applied to synthesize the Neo-CDs using a single substrate, neomycin being a source of carbon as well as nitrogen (Scheme 1). Initially, neomycin sulfate undergoes bond breaking and ring opening upon heating; further, the reaction with water forms acid. Carbonisation of the carbon moiety occurs in the next step followed by aromatization of sp^3 carbon to form CDs. The prepared Neo-CDs exhibit good water solubility and excellent optical and fluorescence properties. Moreover, the as-prepared Neo-CDs have been developed as a selective and sensitive probe for the detection of Fe^{3+} ions in aqueous solution.

2. Experimental details

2.1 Reagents and materials

Metal ions (Fe^{3+}, Cu^{2+}, Ca^{2+}, Ni^{2+}, Co^{2+}, Cd^{2+}, Hg^{2+}, Mn^{2+}, and Cr^{3+}) were used as a chloride salt. Zn^{2+}, Pb^{2+} and Al^{3+} were used as a nitrate salt. Mg^{2+} and Ba^{2+} were used as sulfate salts. All the metal ions and neomycin sulfate were purchased from TCI Chemicals, Hyderabad, India, and were used directly without further purification. Quinine sulfate was obtained from Sigma Aldrich. Pure double distilled water (DDW) was used during all the experiments. UV-vis absorption spectra were recorded on a Shimadzu UV-vis-1800 spectrophotometer, and fluorescence emission spectra were measured on an Agilent Cary Eclipse spectrofluorophotometer. All the sample solutions were maintained at room temperature during the spectrophotometric measurements.

2.2 Synthesis of Neo-CDs

A conventional hydrothermal method was used to synthesize Neo-CDs. The neomycin sulfate as a single precursor (0.2 g) was dissolved in 5 mL of pure DDW and then transferred into a 25 mL Teflon-lined stainless-steel hydrothermal vessel. The reaction mixture was heated at 200 °C for 5 h in a hot air oven. Further, on cooling to room temperature, the resulting solution was centrifuged for 10 minutes at 10 000 rpm to remove a solid deposit. The supernatant liquid was then removed under reduced pressure and dried to obtain a brown solid. The solid product was used for further characterization and applications.

2.3 Detection of metal ions

The detection of metal ions was conducted in DDW at room temperature. The stock solution of Neo-CDs was prepared in ppm and used for the experiments with appropriate dilution in DDW. A 10^{-3} M stock solution of Fe^{3+} ions was prepared in

DDW and used for the experiments with appropriate dilution in DDW. The UV-vis absorption and fluorescence emission spectra of Neo-CDs in DDW were measured in the presence of metal ions. The absorption and emission spectra of Neo-CDs with different metal ions were recorded in 100% aqueous solution at room temperature.

3. Results and discussion

3.1 Characterization of Neo-CDs

The as-synthesized Neo-CDs were well characterized by means of HRTEM to investigate their particle size distribution, shape, and surface morphology. The Neo-CDs were mostly spherical, and nanoparticles were mono-dispersed. The HR-TEM micrograph and the particle size distribution histogram are displayed in Fig. 1. The size of Neo-CDs was well distributed in the narrow size range of 4.5 to 7.8 nm.

Furthermore, infrared spectroscopy (IR) was employed to investigate the functional groups present on the surface of the as-prepared Neo-CDs. Fig. 2a shows the broad band at 3120 cm^{-1} which corresponds to N–H and O–H stretching vibrations.[32,33] The peak at 1722 cm^{-1} could be assigned to the carbonyl group of carboxylic acid. The strong signals at 1612, 1502, and 1402 cm^{-1} are assigned to C=O of the amide group, C=N, and the C=C stretching vibration, respectively.[27,34–37] Moreover, the strong signals at 1205 and 1130 cm^{-1} are due to C–N, C–O, and C–S stretching vibrations.[37–40] The peak at 1047 cm^{-1} is assigned to S=O stretching vibrations, whereas the absorption peak at 862 cm^{-1} is probably due to C–C=S stretching vibrations.[41–43] The IR absorption results show that the Neo-CDs are rich in amino, hydroxyl and carbonyl groups on their surface. The functional groups such as –OH, $–NH_2$, and –COOH present on the surface of Neo-CDs enhance the solubility of Neo-CDs in water.

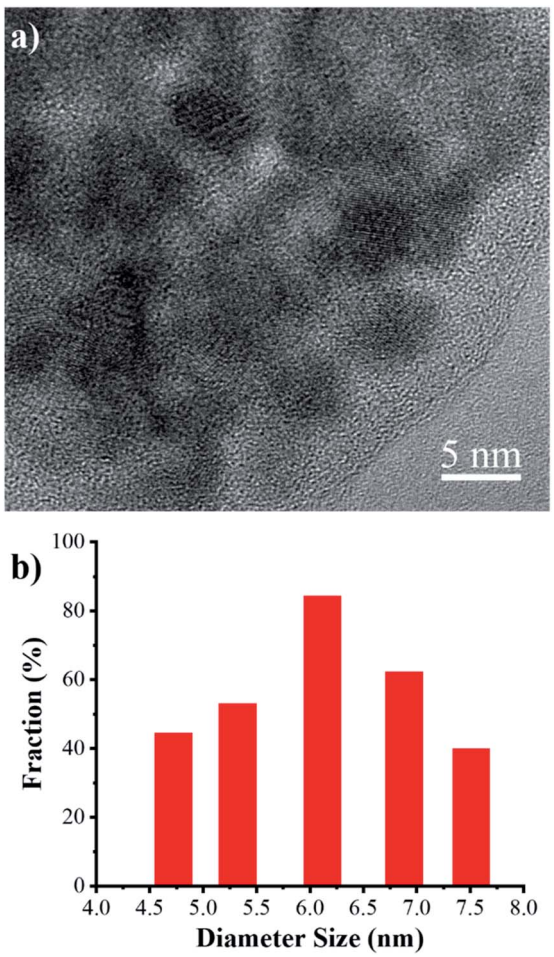

Fig. 1 (a) TEM image and (b) the diameter distribution histogram of the as-prepared Neo-CDs.

Raman spectroscopy is a powerful tool to characterize carbon-based materials. To get structural insights, we further characterized the as-prepared Neo-CDs by Raman spectroscopy. Raman spectroscopy was used to examine the degree of disorder/defects and functional groups in the structure of Neo-CDs. The spectrum of Neo-CDs exhibited two broad bands appearing at 1338 cm^{-1} and 1582 cm^{-1} which correspond to the disordered D band and graphitic G bands, respectively (Fig. 2b). The appearance of these two bands in the Raman spectrum confirmed the presence of carbons dots. The D band derives from the vibrations of carbon atoms with dangling bonds in the termination plane of disordered graphite carbon, while the G band is related to the E_{2g} mode of graphite and vibrations of aromatic sp^2 bonded carbon atoms in the 2-D hexagonal lattice. The calculated relative integrated area of the D band and G band (I_D/I_G) of Neo-CDs was 0.85; the high value of the I_D/I_G ratio suggested that the carbon dots were mainly composed of sp^2 graphitic carbons with sp^3 carbon defects.

Next, X-ray diffraction (XRD) was employed to investigate the crystallinity and purity of Neo-CDs. The as-prepared Neo-CDs exhibited a sharp diffraction pattern, peaks in the 2θ range 20–40° suggesting ordered carbons in Neo-CDs[44] Fig. 2c. The UV-vis absorption and emission behaviour of Neo-CDs have been investigated and are reported in Fig. 2d. The Neo-CDs exhibited a broad absorption band centred at 270 nm, which is mainly due to the π–π* transition of the aromatic π-domain in the carbon dot core. In the fluorescence spectra, an intense emission band was observed at 418 nm (excitation wavelength = 340 nm) in DDW.

XPS measurements were performed to investigate the composition and valence state of elements of the as-prepared Neo-CDs. The XPS spectrum of the Neo-CDs shows peaks at 164.8, 228, 284.5, 397.6, and 528 eV corresponding to binding energy of S_{2p}, S_{2s}, C_{1s}, N_{1s} and O_{1s}, respectively. The chemical compositions of Neo-CDs were C (63.45%), N (7.73%), O (18.98%), and S (9.84%) based on the XPS data (inset in Fig. 3a), disclosing higher sulfur and nitrogen contents. The high resolution XPS spectra of C_{1s} (Fig. 3b) show four peaks with binding energies of about 284.5, 285.3, 285.9, and 288.5 eV. Here, the peak at 284.5 eV is attributed to sp^2 bonding of carbon atoms (C=C); the peak located at 285.3 eV reflects the bonding structure of the C–O/C–N/C–S bonds. The peaks at 285.9 and 288.5 eV are mainly attributed to C=O/C=N and O–C=O bonds, respectively.[18,27,45,46] The high-resolution XPS spectrum of N_{1s} shows three peaks centred at 399.5, 400.8 and 401.5 eV

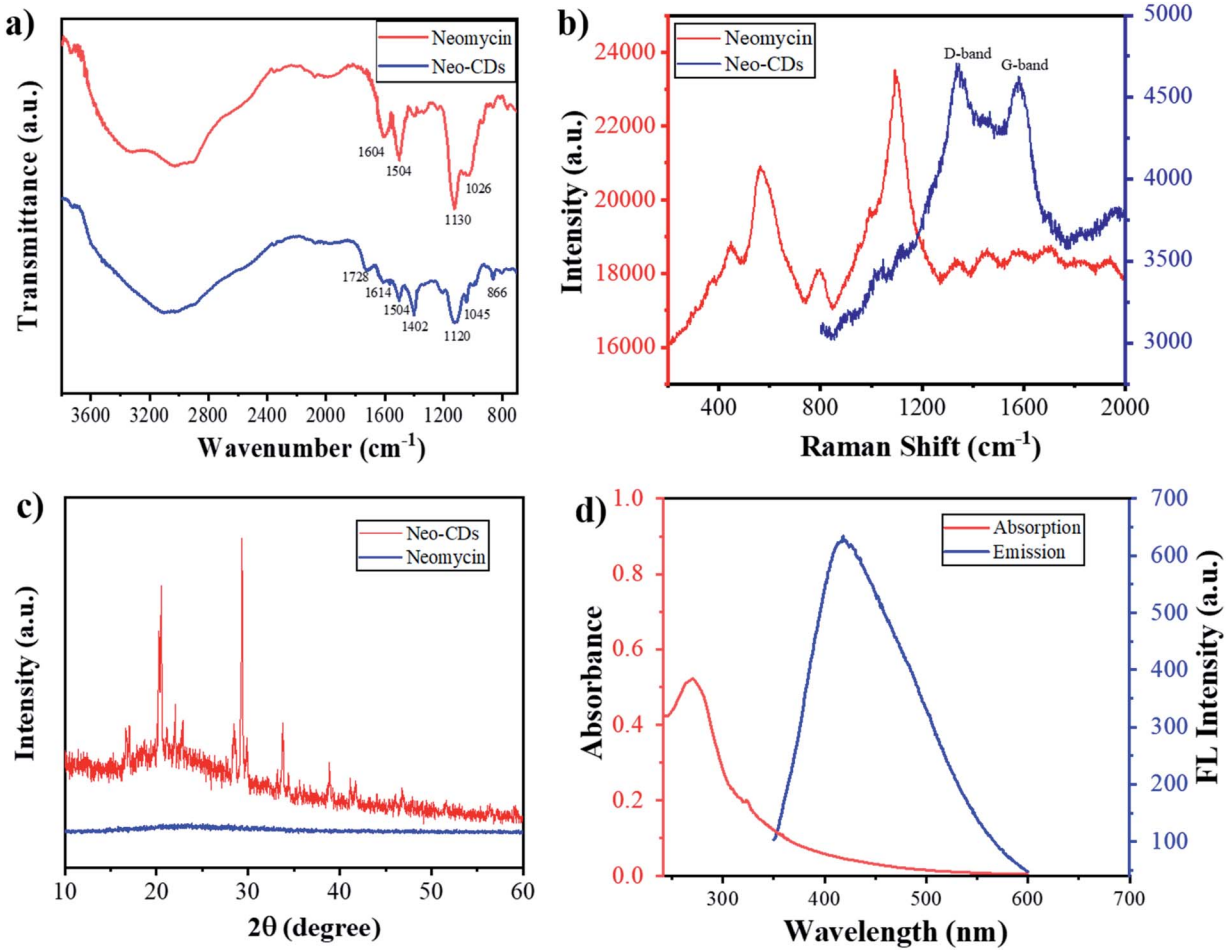

Fig. 2 (a) FTIR spectrum, (b) Raman spectrum, (c) XRD patterns of neomycin and the as-prepared Neo-CDs, and (d) UV-vis absorption and fluorescence spectra in DDW (excitation wavelength = 340 nm).

(Fig. 3c), from which the peak at 399.5 eV reflects the bonding structure of C=N–C bonds.

The second and third peaks at 400.8 and 401.5 eV reflect the bonding structure of the N–H and C–N–C bonds.[16–23] The deconvolution of the O_{1s} region shows three peaks at 530.95, 531.6, and 532.6 eV (Fig. 3d). The peak at 530.95 corresponds to the C=O bond, whereas the peaks at 531.6 and 532.6 eV are mainly attributed to C–OH and C–O–C bonds, respectively.[47–49] The S_{2p} spectrum of Neo-CDs is composed of two peaks centred at 166.8 eV ($S_{2p3/2}$) and 167.9 eV ($S_{2p1/2}$) (Fig. 3e), suggesting that S exists in two forms. These two peaks can be attributed to –C–SO_x ($x = 2, 3, 4$).[50–52] Surface functionality analyses *via* XPS are in good agreement with the FT-IR results. The above analysis indicated that the as-prepared Neo-CDs synthesized have functional groups such as –COOH, –OH, and $–NH_2$.

3.2 Optical properties of the Neo-CDs

The linear optical and fluorescence emission properties of the synthesized Neo-CDs were examined (Fig. 4). The UV-vis absorption spectrum of Neo-CDs exhibits an intense absorption band at 270 nm, which is mainly because of the π–π* transitions of C=C and C=N groups.[53] The broad absorption near 300 nm was attributed to the n–π* transition of the C=O group[33] The UV absorption tails at 400 nm may be assigned to low energy transitions of functional groups attached to the edge of the sp^2 hybridized graphitic carbon core.[54] The synthesized Neo-CDs exhibited bright blue luminescence under 365 nm UV light.

In the solvatochromic study, fluorescence spectra of Neo-CDs have been recorded in various solvents. The Neo-CDs showed different emission behaviours in different solvents as shown in Fig. 4a. Such variations in the fluorescence may be because of the changes in parameters such as size, solvent polarity, and excitation wavelength. The Neo-CDs showed a slight decreased shift in the emission in THF, acetone, DMF and acetonitrile solvents at around 413 nm as compared to DDW, ethanol and DMSO solvents at around 418 nm. Moreover, the highest emission intensity was obtained in DDW at 418 nm compared to other solvents used in the study. This different behaviour is mainly due to the solvatochromic effect and difference in the solvation energy of the ground state and excited state of Neo-CDs in different solvents.

The Neo-CDS exhibited excitation dependent emission spectra; as the excitation wavelengths increased from 300 nm to

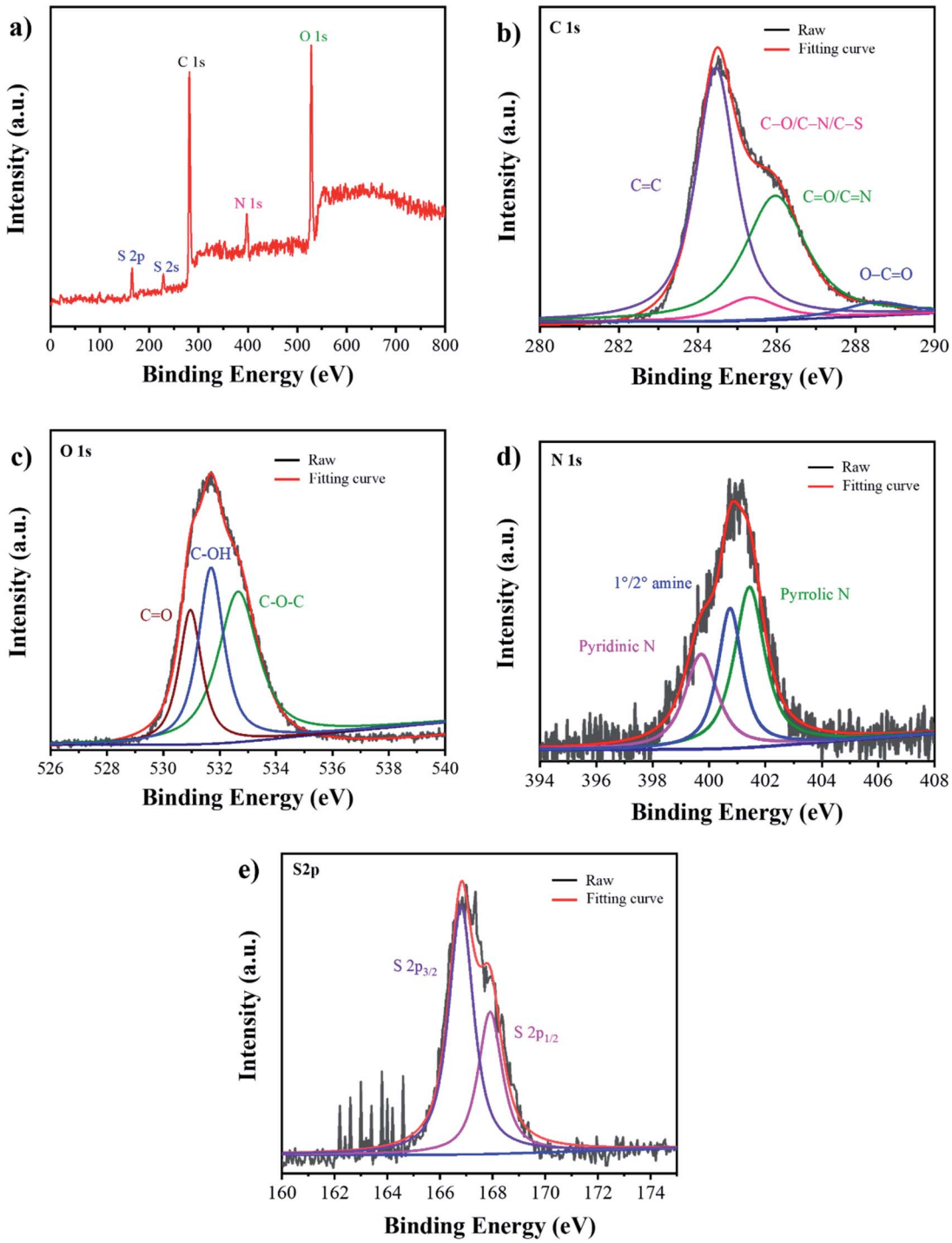

Fig. 3 XPS spectra of (a) survey; (b–e) high resolution C 1s, O 1s, N 1s, and S 2p XPS spectra of Neo-CDs.

500 nm, Neo-CDs showed red shifted emission in DDW (Fig. 4b). The presence of different functional groups on the surface of Neo-CDs produces different energy states upon excitation at different wavelengths of light; therefore, they show emission in different energy states.[55–57] Moreover, this fluorescence behaviour of Neo-CDs may be also due to the presence of different particle sizes and distribution of different surface energy traps of the CDs.[58–61]

The quantum yield (QY) of Neo-CDs was calculated to be 55% in DDW using quinine sulfate as the reference. Furthermore, we have examined the photostability of Neo-CDs. The fluorescence emission intensity had no significant change after continuous irradiation of 365 nm UV light for 100 minutes (Fig. S1a†). The stability of Neo-CDs was also examined under 254 nm UV light, Fig. S1b.† The results suggested that the Neo-CDs possessed excellent photostability under 365 nm UV light and could be

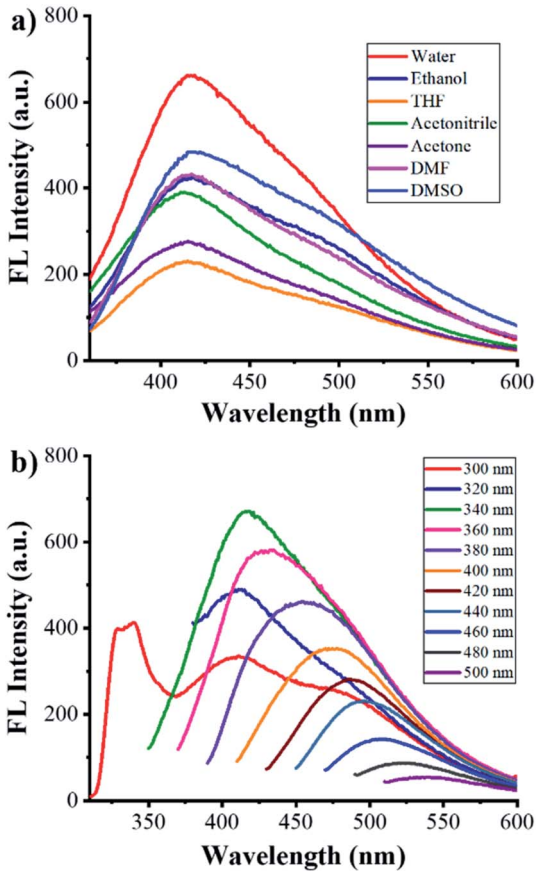

Fig. 4 (a) Fluorescence spectra of Neo-CDs in different solvents (excitation wavelength = 340 nm) and (b) fluorescence spectra in DDW at different excitation wavelengths.

used further for sensing applications under physiological conditions. These attractive properties of Neo-CDs lead to enhancement of their application in sensing. The excellent photoluminescent properties of Neo-CDs such as strong emission, good photostability and high quantum yield are mainly due to the quantum confinement effect (QCE) and edge effect.[62]

3.3 Effect of ionic strength and the masking agent

As shown in Fig. S2a,† the influence of ionic strength on Neo-CDs was examined. The NaCl solutions with various concentrations (0.01–0.25 M) were denoted as the ionic model. 1 mL of the prepared concentrations of 0.05, 0.10, 0.15, 0.20 and 0.25 M NaCl was added into the Neo-CD solution (1 mg mL^{-1}), and their fluorescence spectra were recorded. It was observed that there is no significant increase in the fluorescence intensity with 0.01 to 0.25 M concentrations of NaCl, whereas upon increasing the concentration of NaCl to 0.5 and 1 M, an increase in the fluorescence intensity was observed. Hence, the strength of the ion initiates the electrostatic reaction.[63] With increase in the NaCl concentration, the aggregation of Neo-CDs takes place because of the influence of the electrostatic interactions.[64] Also, the influence of the masking agent on the fluorescence intensity of Neo-CDs was studied with 0.01–0.05 M EDTA (Fig. S2b†). One mL of the prepared concentrations of 0.01, 0.02, 0.03, 0.04, and 0.05 M EDTA was added into the Neo-CD solution (1 mg mL^{-1}), and their fluorescence spectra were recorded. The findings of this investigation specify that there is no effect of the masking agent on the fluorescence intensity of the Neo-CD solution.

3.4 Effect of pH

The fluorescence spectra of Neo-CDs in different pH solutions were recorded to investigate the effect of pH on the fluorescence intensity. The fluorescence intensity was decreased at pH 4 and 7.4 of the phosphate buffer and at 9.2 (Fig. S3†), indicating protonation–deprotonation taking place on the surface of Neo-CDs. Overall, these results suggest that the Neo-CDs were relatively less stable under the conditions.

4. Fluorimetric detection of Fe^{3+}

The fluorometric detection has been proven to be a very easy and attractive tool to evaluate the selectivity of chemo-sensors towards a particular metal ion. The unique luminescent properties of Neo-CDs make them effective sensors for the detection of metal ions, proteins, and macromolecules based on fluorescence turn-on/turn-off mechanisms. In this study, the sensing aptitude of Neo-CDs towards the Fe^{3+} ion was investigated by colorimetric and fluorometric experiments.

4.1 Naked eye detection

The stock solution of Neo-CDs (1 mg mL^{-1}) was prepared by dissolving in DDW. 10 mL of this stock solution was added to a series of metal ions such as $FeCl_3$, $CuCl_2$, $CaCl_2$, $NiCl_2$, $CoCl_2$, $Zn(NO_3)_2$, $CdCl_2$, Mg_2SO_4, $PbSO_4$, $Al(NO_3)_3$, $HgCl_2$, $BaSO_4$, $MnCl_2$, and $CrCl_3$. The sensing performance of Neo-CDs was then monitored by a visual colour change in the UV light (365 nm) and is depicted in Fig. 5. Under 365 nm UV light, the blue fluorescence of the Neo-CDs gets quenched after addition of Fe^{3+} ions, whereas other metal ions did not show such fluorescence quenching. These naked eye results suggested that Neo-CDs act as a fluorescent sensor for the selective detection of the Fe^{3+} ion.

Furthermore, we have studied the sensing aptitude of Neo-CDs using UV-vis absorption and fluorescence emission spectroscopies and also performed competitive experiments to figure out the selectivity of Neo-CDs toward the Fe^{3+} ion.

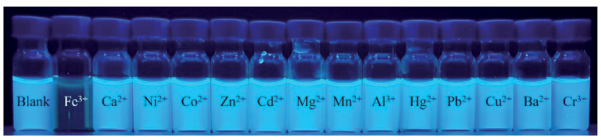

Fig. 5 Solutions of Neo-CDs in DDW with and without the addition of Fe^{3+}, Cu^{2+}, Ca^{2+}, Ni^{2+}, Co^{2+}, Zn^{2+}, Cd^{2+}, Mg^{2+}, Pb^{2+}, Al^{3+}, Hg^{2+}, Ba^{2+}, Mn^{2+}, and Cr^{3+} metal ions under 365 nm UV light.

4.2 UV-vis absorption and fluorescence response of Neo-CDs to Fe^{3+} ions

UV-vis absorption spectroscopy was employed to investigate the selectivity and extent of interactions between Neo-CDs and the metal ions in DDW. The absorption and emission spectra of Neo-CDs were measured in the presence and absence of Fe^{3+} ions as shown in Fig. S4.† The Neo-CDs exhibit an absorbance at about 270 nm, whereas upon addition of Fe^{3+} ions, intensity of the absorption maxima increases. From these results, we conclude that Fe^{3+} ions interact strongly with carboxyl, hydroxyl and amino groups which are present on the surface of Neo-CDs to form a stable complex.

Fluorescence emission spectroscopy was employed to investigate the binding interactions of Neo-CDs with different metal ions in DDW. The Neo-CDs upon excitation at 340 nm exhibited an intense emission peak at 418 nm. The emission band at 418 nm was used to monitor the sensing performance of Neo-CDs with different metal ions. Interestingly, the fluorescence of Neo-CDs was quenched with Fe^{3+} (1.6 μM) Fig. 6a. The feasibility of Neo-CDs has been evaluated towards the detection of Fe^{3+} ions in comparison with different selected metal ions such as Fe^{2+}, Cu^{2+}, Ca^{2+}, Ni^{2+}, Co^{2+}, Zn^{2+}, Cd^{2+}, Mg^{2+}, Pb^{2+}, Al^{3+}, Hg^{2+}, Ba^{2+}, Mn^{2+}, and Cr^{3+}. As shown in Fig. 6b, the fluorescence emission of Neo-CDs at 418 nm was significantly quenched with the Fe^{3+} ion, whereas with other metal ions, there was no obvious change.

Hence, the Neo-CDs showed selective response to Fe^{3+} ions in the system containing different metal ions. It is well known that the Fe^{3+} ion with a half-filled 3d orbital could form effective coordination interactions with various functional groups such as –OH and $–NH_2$ on the surface of Neo-CDs. The photoinduced electron transfer occurs from the excited S1 state of Neo-CDs to the half-filled 3d orbital of the Fe^{3+} ion, resulting in fluorescence quenching through non-radiative transition. From this result, we proposed a possible mechanism of quenching of fluorescence of Neo-CDs by Fe^{3+} ions Fig. 7. This suggests that the mechanism of fluorescence quenching of Neo-CDs by Fe^{3+} ions can be attributed to dynamic quenching. The co-ordination between surface functional groups of Neo-CDs and the Fe^{3+} ion facilitates transfer of abundant electrons from Neo-CDs in the excited state to the 3d orbital of Fe^{3+} and finally causes strong fluorescence quenching. The non-radiative charge transfer complex formation takes place *via* a photoinduced electron transfer process. Furthermore, to get deep insight into the binding ability of Neo-CDs towards Fe^{3+} ions, fluorescence titration experiments were performed with the incremental addition of Fe^{3+} ions (0 to 1.6 μM) in DDW. It was found that the emission intensity peak at 418 nm wavelength decreased from 661 to 49 after addition of 1.6 μM of Fe^{3+} ions. This fluorescence quenching mainly occurs due to photoinduced electron transfer (PET) from Neo-CDs to the Fe^{3+} ion upon complexation of Neo-CDs with the Fe^{3+} ion.

The initial fluorescence intensity of Neo-CDs was found to show a significant decrease upon incremental addition of the Fe^{3+} ion. The fluorescence quenching efficiency (η) was calculated using the equation $[(I_0 - I)/I_0] \times 100\%$, where I_0 and I are the fluorescence intensities before and after addition of the Fe^{3+} ion. After the addition of 1.6 μM of the Fe^{3+} ion solution, the initial emission intensity of Neo-CDs was quenched, and the quenching efficiency (η) was found to be 94%.

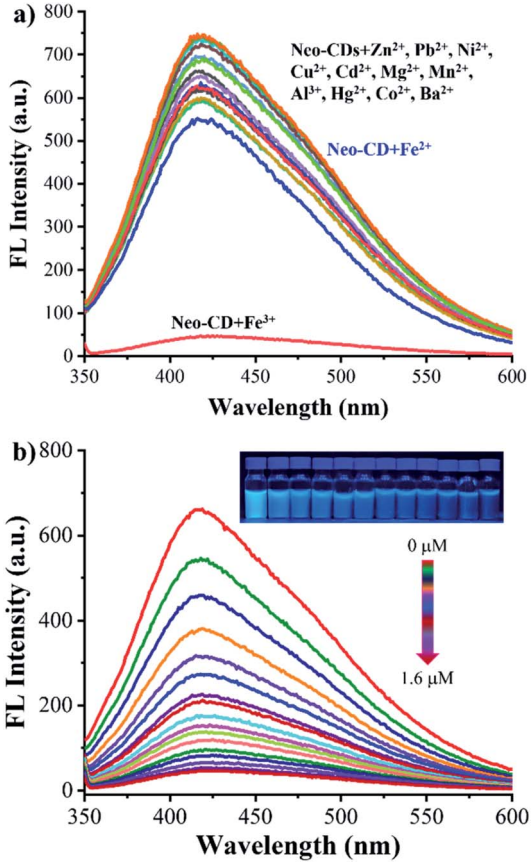

Fig. 6 Emission spectra of Neo-CDs upon excitation at 340 nm wavelength. (a) PL of Neo-CDs with the addition of various metal ions in DDW and (b) PL titration of Neo-CDs with the incremental addition of Fe^{3+} ions in DDW.

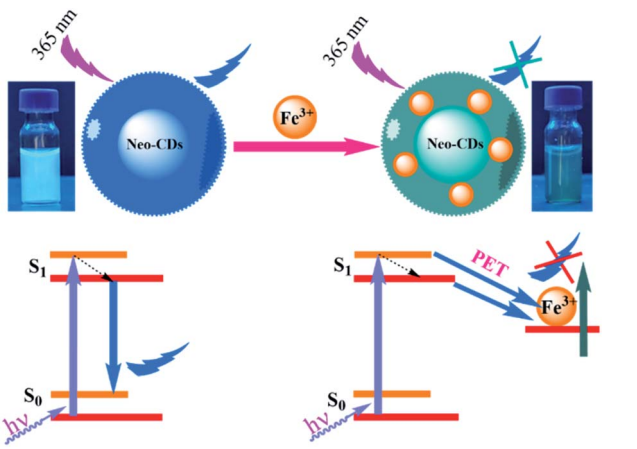

Fig. 7 Fluorescence quenching mechanism of Neo-CDs by Fe^{3+} ions.

4.3 Selectivity study and competitive binding study of Neo-CDs for Fe^{3+} ions

To study the selectivity of Neo-CDs for Fe^{3+} ion detection, the fluorescence response of Neo-CDs with various metal ions such as Cu^{2+}, Ca^{2+}, Ni^{2+}, Co^{2+}, Zn^{2+}, Cd^{2+}, Mg^{2+}, Pb^{2+}, Al^{3+}, Hg^{2+}, Ba^{2+}, Mn^{2+}, and Cr^{3+} have been recorded. The Neo-CDs exhibited significant response (quenching of fluorescence) to the Fe^{3+} ion as compared to other metal ions. The fluorescence response is illustrated in Fig. 8a, which clearly shows that Neo-CDs are selective for the detection of the Fe^{3+} ion. Further, the selectivity of Neo-CDs towards Fe^{3+} in the presence of a variety of interfering metal cations was studied using fluorescence experiments, and the results are displayed in Fig. 8b. The competitive binding experiments of Neo-CDs were carried out by using various metal cations such as Cu^{2+}, Ca^{2+}, Ni^{2+}, Co^{2+}, Zn^{2+}, Cd^{2+}, Mg^{2+}, Pb^{2+}, Al^{3+}, Hg^{2+}, Ba^{2+}, Mn^{2+}, and Cr^{3+}. The interfering metal ions showed similar emission properties to that of the Fe^{3+} ion. Interestingly, the fluorescence of Neo-CDs was quenched upon addition of the Fe^{3+} ion in the presence of interfering metal ions. From these fluorescence results, we conclude that there is no impact of other metal ions on the binding of Neo-CDs with Fe^{3+}. These results confirm that Neo-CDs are very selective towards the detection of Fe^{3+}.

4.4 Stern–Volmer plot and the limit of detection

The Stern–Volmer quenching constant (K_{sv}) was calculated employing fluorescence emission intensity (I_0/I) as a function of increasing Fe^{3+} ion concentration [Q] by using the following relation; I_0/I = Neo-CDs + K_{sv} [Q], where I_0 and I are the emission intensities of Neo-CDs before and after addition of the Fe^{3+} ion, respectively; K_{sv} is the quenching constant (M^{-1}), and [Q] is the molar concentration of the Fe^{3+} ion. The Stern–Volmer plot of Neo-CDs with the Fe^{3+} ion is shown in Fig. 9a. It can be seen that at low concentrations of Fe^{3+} (0.40 μM), the Stern–Volmer plot followed a good linearity, whereas at higher concentrations, the linearity slightly deviated in the upward direction. The positive curvature of the Stern–Volmer plot is mainly attributed to processes such as intersystem crossing, formation of charge transfer complexes at the ground state and excited states as a consequence of both static and dynamic quenching, as well as efficient migration of a singlet exciton.[65] Moreover, the K_{sv} value obtained for the Fe^{3+} ion was 5.6 × 10^6 M^{-1}. The results

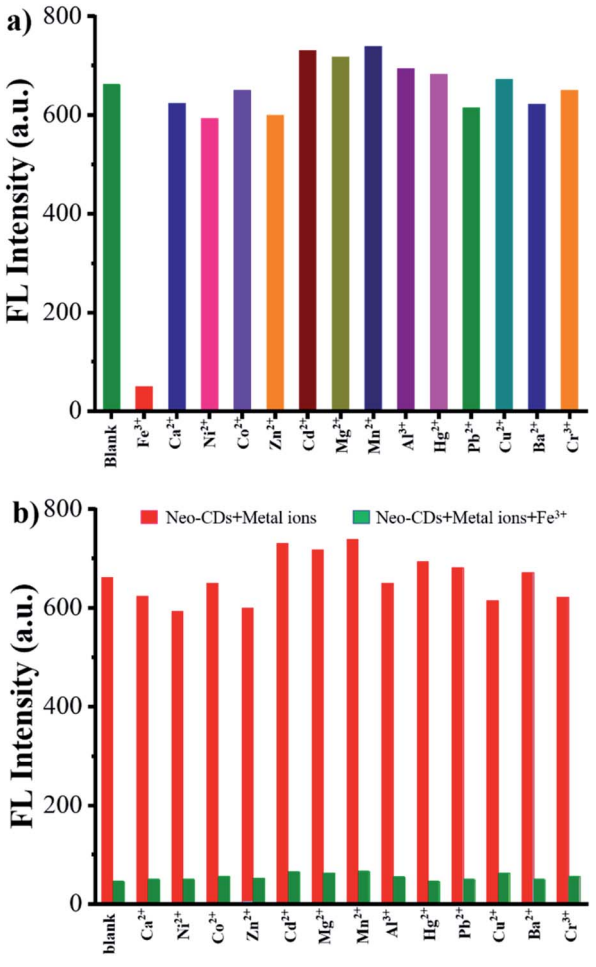

Fig. 8 (a) Fluorescence emission responses of Neo-CDs toward Fe^{3+}, Cu^{2+}, Ca^{2+}, Ni^{2+}, Co^{2+}, Zn^{2+}, Cd^{2+}, Mg^{2+}, Pb^{2+}, Al^{3+}, Hg^{2+}, Ba^{2+}, Mn^{2+}, and Cr^3 metal ions at 418 nm in DDW, (b) pictogram of fluorescence spectra of Neo-CDs exposed to various metal ions and the mixture of Neo-CDs and Fe^{3+} in DDW.

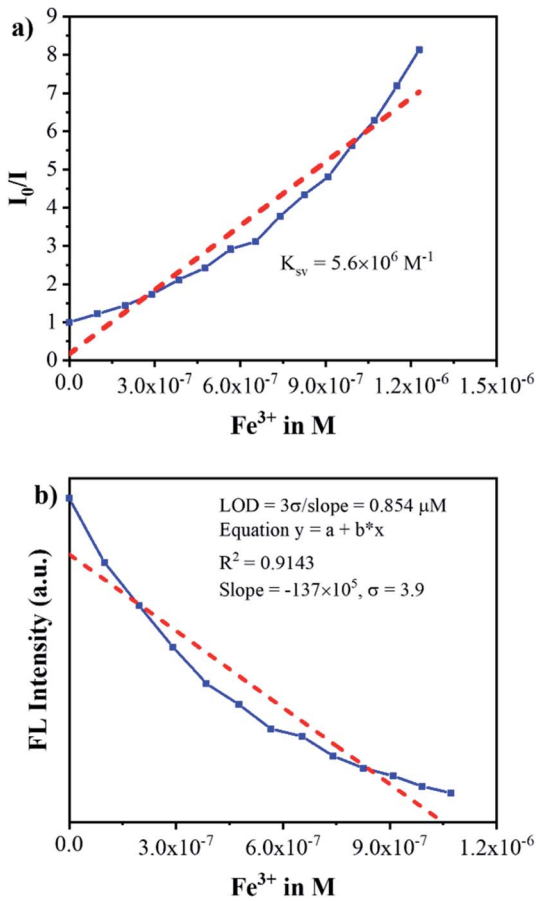

Fig. 9 (a) Stern–Volmer plot for Neo-CDs with the Fe^{3+} ion and (b) plot for the determination of the limit of detection (LOD) for the Fe^{3+} ion.

demonstrated that Fe^{3+} exhibits exclusive quenching ability towards fluorescent Neo-CDs in water.

To evaluate the detection limit, fluorescence titration of Neo-CDs with the Fe^{3+} ion was done with increasing concentrations of the Fe^{3+} ion, and the emission intensity as a function of the Fe^{3+} ion concentration was plotted (Fig. 9b). Upon increasing the Fe^{3+} concentration from 0.01 to 0.40 μM, fluorescence intensity of Neo-CDs linearly decreased and slightly curved in the upward direction at 0.40 μM. The difference in the fluorescence intensity of Neo-CDs before and after adding Fe^{3+} was proportional to the concentration of Fe^{3+}. The LOD plot showed linear regions over the range of 0–0.40 μM, indicating that Neo-CDs and the Fe^{3+} ion are in good linear relationship with each other. The detection limit was calculated from the fluorescence titrations by using equation $3\sigma/m$, where σ is the standard deviation of the emission of the free Neo-CD sensor, and m is the slope from the plot. The detection limit of Neo-CDs for the Fe^{3+} ion was found to be as low as 0.854 μM, which is comparatively lower than those of most of the other fluorescent probes for the Fe^{3+} ion (Table S2†). These results clearly prove that Neo-CDs have great potential to detect the Fe^{3+} ion, selectively.

5. Conclusions

In summary, Neo-CDs with high fluorescence quantum yield (55%) were synthesized for the first-time using the neomycin antibiotic as a single precursor *via* a simple hydrothermal method. It was found that the spherical Neo-CDs have an average size of 4.5 to 7.8 nm as well as good dispersity in solution. The as-prepared Neo-CDs have been proved to have favourable ionic strength, high stability under 365 nm UV light, excellent water solubility and excitation dependent fluorescence emission. Neo-CDs without any modification or purification have been demonstrated as a sensor and showed high selectivity and sensitivity towards the Fe^{3+} ion. Most importantly, these Neo-CDs provided a rapid, reliable, and fluorescence turn-off method for detection of Fe^{3+} with a detection limit of 0.854 μM. Once the Fe^{3+} ion was added to Neo-CD solutions, the PL intensities of the Neo-CDs were significantly quenched. A possible mechanism of quenching of fluorescence of Neo-CDs by the Fe^{3+} ion is proposed to be due to the complexation of Neo-CDs and the Fe^{3+} ion. The effective co-ordination of –OH and $-NH_2$ groups with the Fe^{3+} ion on the surface of Neo-CDs leads to complex formation. The quenching efficiency and Stern–Volmer quenching constant were calculated and found to be 94% and 5.6×10^6 M^{-1}, respectively. These results clearly demonstrated that Neo-CDs can be used as an efficient sensor for the selective detection of Fe^{3+} ions is water.

Author contributions

R. W. J. performed the characterization and sensing applications of Neo-CDs and data interpretation, along with manuscript preparation. P. P. K. performed the synthesis of Neo-CDs and helped in their characterization. S. T. B. guided P. P. K. and corrected the manuscript. S. V. B. analysed the data and finalized the manuscript. All co-authors reviewed the manuscript.

Conflicts of interest

The authors declare no competing interests.

Acknowledgements

R. W. J. acknowledges joint CSIR-UGC for a NET Senior Research Fellowship. S. V. B. acknowledges UGC-FRP for financial support and Professorship, and we also acknowledge the Council of Scientific & Industrial Research (CSIR), New Delhi, India, for providing support under project code No. 02(0357)/19/EMR-II.

References

1 B. Becker and M. A. Cooper, *ACS Chem. Biol.*, 2013, **8**, 105–115.
2 T. Hermann, *Cell. Mol. Life Sci.*, 2007, **64**, 1841–1852.
3 F. Paquin, J. Rivnay, A. Salleo, N. Stingelin and C. Silva, *J. Mater. Chem. C*, 2015, **3**, 10715–10722.
4 R. W. Jadhav, M. Al Kobaisi, L. A. Jones, A. Vinu and S. V. Bhosale, *ChemistryOpen*, 2019, **8**, 1154–1166.
5 J. Hu, L. Yang, X. Cheng, Y. Li and Y. Cheng, *Adv. Funct. Mater.*, 2021, **31**, 2103718.
6 N. T. Chandrika, K. D. Green, J. L. Houghton and S. Garneau-Tsodikova, *ACS Med. Chem. Lett.*, 2015, **6**, 1134–1139.
7 N. N. Degtyareva, C. Gong, S. Story, N. S. Levinson, A. K. Oyelere, K. D. Green, S. Garneau-Tsodikova and D. P. Arya, *ACS Infect. Dis.*, 2017, **3**, 206–215.
8 R. W. Jadhav, D. D. La, V. G. More, H. Tung Vo, D. A. Nguyen, D. L. Tran and S. V. Bhosale, *Sci. Rep.*, 2020, **10**, 1–8.
9 R. W. Jadhav, S. M. Wagalgave, V. Bajarang and R. M. Khadake, *Sci. Rep.*, 2022, **12**, 1–10.
10 O. A. Sadik, S. K. Mwilu and A. Aluoch, *Electrochim. Acta*, 2010, **55**, 4287–4295.
11 B. K. Walther, C. Z. Dinu, D. M. Guldi, V. G. Sergeyev, S. E. Creager, J. P. Cooke and A. Guiseppi-Elie, *Mater. Today*, 2020, **39**, 23–46.
12 V. D. Krishna, K. Wu, D. Su, M. C. J. Cheeran, J. P. Wang and A. Perez, *Food Microbiol.*, 2018, **75**, 47–54.
13 T. Dertinger, R. Colyer, R. Vogel, M. Heilemann, M. Sauer, J. Enderlein and S. Weiss, *Adv. Exp. Med. Biol.*, 2012, **733**, 17–21.
14 H. Liu, Q. Wang, G. Shen, C. Zhang, C. Li, W. Ji, C. Wang and D. Cui, *Nanoscale Res. Lett.*, 2014, **9**, 1–11.
15 S. Pandit, T. Banerjee, I. Srivastava, S. Nie and D. Pan, *ACS Sens.*, 2019, **4**, 2730–2737.
16 H. Ali, S. Ghosh and N. R. Jana, *MRS Adv.*, 2018, **3**, 779–788.
17 K. Ariga, *Nanoscale Horiz.*, 2021, **6**, 364–378.
18 X. Chen, J. Bai, Y. Ma, G. Yuan, J. Mei, L. Zhang and L. Ren, *Microchem. J.*, 2019, **149**, 103981.
19 Q. Xu, P. Pu, J. Zhao, C. Dong, C. Gao, Y. Chen, J. Chen, Y. Liu and H. Zhou, *J. Mater. Chem. A*, 2015, **3**, 542–546.

20 M. Ozhukil Valappil, S. Alwarappan and V. K. Pillai, *Nanoscale*, 2022, **14**, 1037–1053.
21 N. Sohal, B. Maity and S. Basu, *RSC Adv.*, 2021, **11**, 25586–25615.
22 F. J. Cao, L. Wang, C. L. Feng, X. Lin and H. Feng, *RSC Adv.*, 2021, **11**, 34174–34180.
23 M. Moradi, A. Vaskin, I. Staude, M. Jäger, J. Elbert and U. S. Schubert, *ACS Appl. Nano Mater.*, 2021, **4**, 2386–2394.
24 B. Shi, Y. Su, L. Zhang, M. Huang, R. Liu and S. Zhao, *ACS Appl. Mater. Interfaces*, 2016, **8**, 10717–10725.
25 T. Song, Q. Wang, H. Yu, W. Gao, Y. Xu, Y. Lv, Y. Xing, Y. Chen and M. Yang, *Anal. Bioanal. Chem.*, 2022, **414**, 1623–1630.
26 C. Guo, A. C. Sedgwick, T. Hirao and J. L. Sessler, *Coord. Chem. Rev.*, 2021, **427**, 213560.
27 Y. Dong, J. Cai, X. You and Y. Chi, *Analyst*, 2015, **140**, 7468–7486.
28 A. Pramanik, S. Biswas and P. Kumbhakar, *Spectrochim. Acta, Part A*, 2018, **191**, 498–512.
29 Z. Xu, X. Wang, X. Liu, Z. Cui, X. Yang, K. W. K. Yeung, J. C. Chung, P. K. Chu and S. Wu, *ACS Appl. Mater. Interfaces*, 2017, **9**, 39657–39671.
30 S. Bhandari, D. Mondal, S. K. Nataraj and R. G. Balakrishna, *Nanoscale Adv.*, 2019, **1**, 913–936.
31 Ł. Janus, J. Radwan-Pragłowska, M. Piatkowski and D. Bogdał, *Materials*, 2020, **13**, 3313.
32 Z. Yang, M. Xu, Y. Liu, F. He, F. Gao, Y. Su, H. Wei and Y. Zhang, *Nanoscale*, 2014, **6**, 1890–1895.
33 X. Teng, C. Ma, C. Ge, M. Yan, J. Yang, Y. Zhang, P. C. Morais and H. Bi, *J. Mater. Chem. B*, 2014, **2**, 4631–4639.
34 S. Chandra, D. Bano, K. Sahoo, D. Kumar, V. Kumar, P. Kumar Yadav and S. Hadi Hasan, *Microchem. J.*, 2022, **172**, 106953.
35 A. Dager, T. Uchida, T. Maekawa and M. Tachibana, *Sci. Rep.*, 2019, **9**, 1–10.
36 Z. Feng, Z. Li, X. Zhang, Y. Shi and N. Zhou, *Molecules*, 2017, **22**, 2061.
37 X. Shao, H. Gu, Z. Wang, X. Chai, Y. Tian and G. Shi, *Anal. Chem.*, 2013, **85**, 418–425.
38 H. Ding, P. Zhang, T. Y. Wang, J. L. Kong and H. M. Xiong, *Nanotechnology*, 2014, **25**, 205604.
39 S. Zhu, K. Wang, J. Hu, R. Liu and H. Zhu, *Materials Advances*, 2020, **1**, 3176–3181.
40 H. Liu, Y. Zhang and C. Huang, *J. Pharm. Anal.*, 2019, **9**, 127–132.
41 J. Mondal, V. Revuri, P. Choochana, P. Ganesan, W. J. Kang and Y. kyu Lee, *J. Pharm. Invest.*, 2020, **50**, 209–218.
42 H. Ding, J. S. Wei and H. M. Xiong, *Nanoscale*, 2014, **6**, 13817–13823.
43 H. Lu, C. Li, H. Wang, X. Wang and S. Xu, *ACS Omega*, 2019, **4**, 21500–21508.
44 Q. Zhang, S. Xie, Y. Yang, Y. Wu, X. Wang, J. Wu, L. Zhang, J. Chen and Y. Wang, *J. Anal. Methods Chem.*, 2018, 7890937.
45 S. Bian, C. Shen, H. Hua, L. Zhou, H. Zhu, F. Xi, J. Liu and X. Dong, *RSC Adv.*, 2016, **6**, 69977–69983.
46 M. Vedamalai, A. P. Periasamy, C. W. Wang, Y. T. Tseng, L. C. Ho, C. C. Shih and H. T. Chang, *Nanoscale*, 2014, **6**, 13119–13125.
47 P. Ni, Q. Li, C. Xu, H. Lai, Y. Bai and T. Chen, *Appl. Surf. Sci.*, 2019, **494**, 377–383.
48 G. He, Y. Zhang and Q. He, *Catalysts*, 2019, **9**, 19–21.
49 A. Abdul Razzaq, Y. Yao, R. Shah, P. Qi, L. Miao, M. Chen, X. Zhao, Y. Peng and Z. Deng, *Energy Storage Materials*, 2019, **16**, 194–202.
50 S. Yang, L. Zhi, K. Tang, X. Feng, J. Maier and K. Müllen, *Adv. Funct. Mater.*, 2012, **22**, 3634–3640.
51 Y. Li, J. Wang, X. Li, D. Geng, M. N. Banis, Y. Tang, D. Wang, R. Li, T. K. Sham and X. Sun, *J. Mater. Chem.*, 2012, **22**, 20170–20174.
52 S. Graphene, M. C. Catalyst and O. Reduction, *ACS Nano*, 2012, **6**, 205–211.
53 X. Sun, C. Brückner and Y. Lei, *Nanoscale*, 2015, **7**, 17278–17282.
54 F. Liu, M. H. Jang, H. D. Ha, J. H. Kim, Y. H. Cho and T. S. Seo, *Adv. Mater.*, 2013, **25**, 3657–3662.
55 D. Pan, J. Zhang, Z. Li and M. Wu, *Adv. Mater.*, 2010, **22**, 734–738.
56 A. Jaiswal, S. Sankar Ghosh and A. Chattopadhyay, *Chem. Commun.*, 2012, **48**, 407–409.
57 S. N. Baker and G. A. Baker, *Angew. Chem., Int. Ed.*, 2010, **49**, 6726–6744.
58 Y. Dong, H. Pang, H. Bin Yang, C. Guo, J. Shao, Y. Chi, C. M. Li and T. Yu, *Angew. Chem., Int. Ed.*, 2013, **52**, 7800–7804.
59 Y. P. Sun, B. Zhou, Y. Lin, W. Wang, K. A. S. Fernando, P. Pathak, M. J. Meziani, B. A. Harruff, X. Wang, H. Wang, P. G. Luo, H. Yang, M. E. Kose, B. Chen, L. M. Veca and S. Y. Xie, *J. Am. Chem. Soc.*, 2006, **128**, 7756–7757.
60 R. Liu, D. Wu, S. Liu, K. Koynov, W. Knoll and Q. Li, *Angew. Chem., Int. Ed.*, 2009, **48**, 4598–4601.
61 B. De, M. Kumar, B. B. Mandal and N. Karak, *RSC Adv.*, 2015, **5**, 74692–74704.
62 F. Zhang, Y. Zheng, J. Liang, S. Long, X. Chen and K. Tan, *Spectrochim. Acta, Part A*, 2016, **159**, 7–12.
63 B. A. Humphreys, E. J. Wanless and G. B. Webber, *J. Colloid Interface Sci.*, 2018, **516**, 153–161.
64 Q. Hu, X. Gong, L. Liu and M. M. F. Choi, *J. Nanomater.*, 2017, **2017**, 30–37.
65 B. Prusti and M. Chakravarty, *Analyst*, 2020, **145**, 1687–1694.

